

The galaxy major merger fraction to $z \sim 1$

Carlos López-Sanjuan¹, Marc Balcells¹, Pablo G. Pérez-González², Guillermo Barro², César Enrique García-Dabó^{1,3},
Jesús Gallego², and Jaime Zamorano²

¹ Instituto de Astrofísica de Canarias, Calle Vía Láctea s/n, E-38205 La Laguna, Tenerife, Spain

² Departamento de Astrofísica y Ciencias de la Atmósfera, Facultad de C.C. Físicas, Universidad Complutense de Madrid, E-28040 Madrid, Spain

³ European South Observatory, Karl-Schwarzschild-Strasse 2, D-85748 Garching, Germany

Received 23 February 2009; Accepted 12 May 2009

ABSTRACT

Aims. The importance of disc–disc major mergers in galaxy evolution remains uncertain. We study the major merger fraction in a SPITZER/IRAC-selected catalogue in the GOODS-S field up to $z \sim 1$ for luminosity- and mass-limited samples.

Methods. We select disc–disc merger remnants on the basis of morphological asymmetries/distortions, and address three main sources of systematic errors: (i) we explicitly apply morphological K-corrections, (ii) we measure asymmetries in galaxies artificially redshifted to $z_d = 1.0$ to deal with loss of morphological information with redshift, and (iii) we take into account the observational errors in z and A , which tend to overestimate the merger fraction, though use of maximum likelihood techniques.

Results. We obtain morphological merger fractions (f_m^{mph}) below 0.06 up to $z \sim 1$. Parameterizing the merger fraction evolution with redshift as $f_m^{\text{mph}}(z) = f_m^{\text{mph}}(0)(1+z)^m$, we find that $m = 1.8 \pm 0.5$ for $M_B \leq -20$ galaxies, while $m = 5.4 \pm 0.4$ for $M_* \geq 10^{10} M_\odot$ galaxies. When we translate our merger fractions to merger rates ($\mathfrak{R}_m^{\text{mph}}$), their evolution, parameterized as $\mathfrak{R}_m^{\text{mph}}(z) = \mathfrak{R}_m^{\text{mph}}(0)(1+z)^n$, is quite similar in both cases: $n = 3.3 \pm 0.8$ for $M_B \leq -20$ galaxies, and $n = 3.5 \pm 0.4$ for $M_* \geq 10^{10} M_\odot$ galaxies.

Conclusions. Our results imply that only $\sim 8\%$ of today's $M_* \geq 10^{10} M_\odot$ galaxies have undergone a disc–disc major merger since $z \sim 1$. In addition, $\sim 21\%$ of $M_* \geq 10^{10} M_\odot$ galaxies at $z \sim 1$ have undergone one of these mergers since $z \sim 1.5$. This suggests that disc–disc major mergers are not the dominant process in the evolution of $M_* \geq 10^{10} M_\odot$ galaxies since $z \sim 1$, with only 0.2 disc–disc major mergers per galaxy, but may be an important process at $z > 1$, with ~ 1 merger per galaxy at $1 < z < 3$.

Key words. Galaxies:evolution — Galaxies:formation — Galaxies:interactions

1. INTRODUCTION

The colour–magnitude diagram of local galaxies shows two distinct populations: the red sequence, consisting primarily of old, spheroid-dominated, quiescent galaxies, and the blue cloud, formed primarily by spiral and irregular star-forming galaxies (Strateva et al. 2001; Baldry et al. 2004). This bimodality has been traced at increasingly higher redshifts (Bell et al. 2004, up to $z \sim 1$; Arnouts et al. 2007; Cirasuolo et al. 2007, up to $z \sim 1.5$; Giallongo et al. 2005; Cassata et al. 2008, up to $z \sim 2$; Kriek et al. 2008, at $z \sim 2.3$). More massive galaxies were the first to populate the red sequence as a result of the so-called “downsizing” (Cowie et al. 1996): massive galaxies experienced most of their star formation at early times and are passive by $z \sim 1$, while many of the less massive galaxies have extended star formation histories (see Bundy et al. 2006; Scarlata et al. 2007; Pérez-González et al. 2008, and references therein).

These results pose a challenge to the popular hierarchical Λ -CDM models, in which one expects that the more massive dark matter halos are the final stage of successive minor halo mergers. However, the treatment of the baryonic component is still unclear. The latest models, which include radiative cooling, star formation, and AGN and supernova feedback, seem to reproduce the observational trends better (see Bower et al. 2006; De Lucia & Blaizot 2007; Stewart et al. 2009; Hopkins et al. 2009b, and references therein). Within this framework, the role of galaxy mergers in the build-up of the red sequence and their

relative importance in the evolution of galaxy properties, i.e. colour, mass, or morphology, is an important open question.

The merger fraction, f_m , defined as the ratio between the number of merger events in a sample and the total number of sources in the same sample, is a useful observational quantity for answering that question. Many studies have determined the merger fraction and its evolution with redshift, usually parameterized as $f_m(z) = f_m(0)(1+z)^m$, using different sample selections and methods, such as morphological criteria (Conselice et al. 2003, 2008, 2009; Lavery et al. 2004; Cassata et al. 2005; Lotz et al. 2008a; Bridge et al. 2007; Kampczyk et al. 2007; Jogee et al. 2009), kinematic close companions (Patton et al. 2000, 2002; Patton & Atfield 2008; Lin et al. 2004, 2008; De Propriis et al. 2005, 2007; Bluck et al. 2009), spatially close pairs (Le Fèvre et al. 2000; Bundy et al. 2004, 2009; Bridge et al. 2007; Kartaltepe et al. 2007; Hsieh et al. 2008), or the correlation function (Bell et al. 2006b; Masjedi et al. 2006). In these studies the value of the merger index m at redshift $z \lesssim 1$ varies in the range $m = 0\text{--}4$. Λ -CDM models predict $m \sim 2\text{--}3$ (Kolatt et al. 1999; Governato et al. 1999; Gottlöber et al. 2001; Fakhouri & Ma 2008) for dark matter halos, while suggesting a weaker evolution, $m \sim 0\text{--}2$, for the galaxy merger fraction (Berrier et al. 2006; Stewart et al. 2008).

To constrain the role of disc–disc major mergers in galaxy evolution, in this paper we study their redshift evolution up to $z \sim 1$ in a SPITZER/IRAC-selected catalogue of the GOODS-S area. We use morphological criteria, based on the fact that, just after a merger is complete, the galaxy image shows strong geomet-

rical distortions, particularly asymmetric distortions (Conselice 2003). Hence, high values in the automatic asymmetry index A (Abraham et al. 1996; Conselice et al. 2000) are assumed to identify disc–disc major merger systems. This methodology presents several systematic effects, such as signal-to-noise dependence (Conselice 2003; Conselice et al. 2005) or contamination by non-interacting galaxies with high asymmetry values (Jogee et al. 2009; Miller et al. 2008), which lead to biased merger fractions if not treated carefully. In a previous study of the Groth field, López-Sanjuan et al. (2009, L09 hereafter) demonstrated a robust procedure to determine morphological merger fractions (f_m^{mph}) using galaxy asymmetries. In that study they avoid the loss of information with redshift by artificially moving all sources to a common redshift, while the experimental error bias, which tends to overestimate the merger fraction up to 50%, was addressed through use of a maximum likelihood method developed in López-Sanjuan et al. (2008, LGB08 hereafter). L09 find that the merger rate decreases with stellar mass at $z = 0.6$, and that 20–35% of present-day $M_B \leq -20$ galaxies have undergone a disc–disc major merger since $z \sim 1$.

This paper is organized as follows: in Sect. 2 we summarize the GOODS-S data set that we use in our study, and in Sect. 3 we develop the asymmetry index calculations and study their variation with redshift. Then, in Sect. 4 we use the methodology to obtain the morphological merger fraction by taking into account the observational errors. In Sect. 5 we summarize the obtained merger fractions and their evolution with z , while in Sect. 6 we compare our results with other authors. Finally, in Sect. 7 we present our conclusions. We use $H_0 = 70 \text{ km s}^{-1} \text{ Mpc}^{-1}$, $\Omega_M = 0.3$, and $\Omega_\Lambda = 0.7$ throughout. All magnitudes are Vega unless noted otherwise.

2. DATA

2.1. The GOODS-S SPITZER/IRAC-selected catalogue

This work is based on the analysis of the structural parameters of the galaxies catalogued in the GOODS-South field by the Spitzer Legacy Team (see Giavalisco et al. 2004). We used the Version 1.0 catalogues¹ and reduced mosaics in the $F435W$ (B_{435}), $F606W$ (V_{606}), $F775W$ (i_{775}), and $F850LP$ (z_{850}) HST/ACS bands. These catalogues were cross-correlated using a $1.5''$ search radius with the GOODS-S IRAC-selected sample in the Rainbow Cosmological Database published in Pérez-González et al. (2008, see also Pérez-González et al. 2005 and Barro et al. 2009, in prep.), which provided us with spectral energy distributions (SEDs) in the UV-to-MIR range, well-calibrated and reliable photometric redshifts, stellar masses, star formation rates and rest-frame absolute magnitudes.

We refer the reader to the above-mentioned papers for a more detailed description of the data included in the SEDs and the analysis procedure. Here, we summarize briefly the main characteristics of the data set. We measured consistent aperture photometry in several UV, optical, NIR and MIR bands with the method described in Pérez-González et al. (2008). UV-to-MIR SEDs were built for all IRAC sources in the GOODS-S region down to a 75% completeness magnitude $[3.6] = 23.5 \text{ mag}$ (AB). These SEDs were fitted to stellar population and dust emission models to obtain an estimate of the photometric redshift (z_{phot}), the stellar mass (M_\star), and the rest-frame absolute B-band magnitude (M_B).

The median accuracy of the photometric redshifts at $z < 1.5$ is $|z_{\text{spec}} - z_{\text{phot}}|/(1 + z_{\text{spec}}) = 0.04$, with a fraction $< 5\%$ of catastrophic outliers (Pérez-González et al. 2008, Fig. B2). Rest-frame absolute B-band magnitudes were estimated for each source by convolving the templates fitting the SED with the transmission curve of a typical Bessel B filter, taking into account the redshift of each source. This procedure provided us with accurately interpolated B -band magnitudes including a robustly estimated k -correction. Stellar masses were estimated using exponential star formation PEGASE01 models with a Salpeter (1955) IMF and various ages, metallicities and dust contents included. The typical uncertainties in the stellar masses are a factor of ~ 2 (typical of any stellar population study; see, e.g., Papovich et al. 2006, Fontana et al. 2006).

Finally, our methodology requires the errors in z_{phot} to be Gaussian (Sect. 4, LGB08, L09), while z_{phot} confidence intervals given by χ^2 methods do not correlate with the differences between z_{spec} 's and z_{phot} 's (Oyaizu et al. 2008). Because of this, and following L09, we use $\sigma_{z_{\text{phot}}} = \sigma_{\delta_z}(1 + z_{\text{phot}})$ as the z_{phot} error, where σ_{δ_z} is the standard deviation in the distribution of the variable $\delta_z \equiv (z_{\text{phot}} - z_{\text{spec}})/(1 + z_{\text{phot}})$, which is well described by a Gaussian with mean $\mu_{\delta_z} \sim 0$ and standard deviation σ_{δ_z} . We found that σ_{δ_z} increases with redshift, and we took $\sigma_{\delta_z} = 0.043$ for $z \leq 0.9$ sources and $\sigma_{\delta_z} = 0.05$ for $z > 0.9$ sources. This procedure assigns the same error to sources with equal z_{phot} , but it is statistically representative of our sample and ensures the best Gaussian approximation of z_{phot} errors in the merger fraction determination (Sect. 4).

2.2. Luminosity- and mass-selected samples

The aim of this study is to determine the galaxy merger fraction in B -band luminosity- and stellar mass-selected samples. The B -band study is motivated by previous studies, which usually selected their samples in that band. This permits us to compare our results with other authors (Sect. 6.2). Moreover, the stellar mass is a fundamental galaxy property that correlates with colour (Baldry et al. 2004) and morphology (Conselice 2006a).

To determine the luminosity limit in the B -band we calculated the third quartile of the M_B source distribution at different redshifts, taking this as a limiting magnitude (e.g., Pérez-González et al. 2008). In the upper panel of Fig. 1 we show M_B vs redshift up to $z_{\text{max}} = 1.3$ (grey dots) and the limiting magnitude at different redshifts (black bullets). The upper redshift limit in our study, $z_{\text{max}} = 1.3$, is fixed by the reliability of the asymmetry index as a morphological indicator without performing morphological K -corrections (see Sect. 3.1.2, for details). The black solid curve is the least-squares fit of the limiting magnitudes by a third-degree polynomial. At redshift $z_{\text{max}} = 1.3$, $M_{B,\text{lim}} \sim -19.5$, so we selected for our study sources with $M_B \leq -19.5$.

We took as limiting mass at each redshift the stellar mass for which the IRAC catalogue is 75% complete for passively evolving galaxies (see Pérez-González et al. 2008). In the lower panel of Fig. 1 we show $\log(M_\star/M_\odot)$ vs redshift up to $z_{\text{max}} = 1.3$ (grey dots) and the 75% of completeness at different redshifts (black bullets). The black solid curve is the least-squares fit of the completeness points by a power-law function. At redshift $z_{\text{max}} = 1.3$, $\log(M_{\star,\text{lim}}/M_\odot) \sim 9.8$, so we selected sources with $M_\star \geq 10^{10} M_\odot$ for our study.

¹ <http://archive.stsci.edu/prepds/goods/>

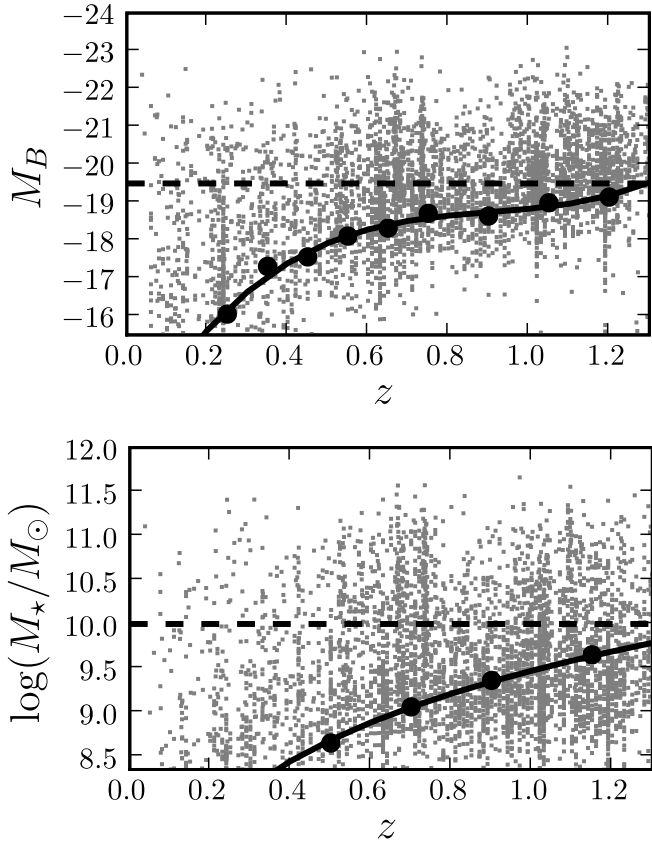


Fig. 1. *Top:* distribution of M_B vs redshift for IRAC catalogue sources. The black dots are the limiting magnitude of the survey at each redshift, defined as the third quartile in magnitude distributions. The solid black curve is the best fit of the limiting magnitude points by a third-degree polynomial. The black dashed line shows the $M_B = -19.5$ limit of our study. *Bottom:* distribution of $\log(M_*/M_\odot)$ vs redshift for IRAC catalogue sources. The black solid curve shows the stellar mass above which the sample is 75% complete for passively evolving galaxies (Pérez-González et al. 2008). The black dashed line shows the $\log(M_*/M_\odot) = 10$ limit of our study.

3. ASYMMETRY INDEX

The automatic asymmetry index (A) is one of the CAS morphological indices (Conselice 2003). This index is defined as

$$A = \frac{\sum |I_0 - I_{180}|}{\sum |I_0|} - \frac{\sum |B_0 - B_{180}|}{\sum |B_0|}, \quad (1)$$

where I_0 and B_0 are the original galaxy and background images, I_{180} and B_{180} are the original galaxy and background images rotated 180 degrees, and the summation spans all the pixels of the images. The background image is defined in detail in the next section. For further details on the asymmetry calculation see Conselice et al. (2000). This index gives us information over the source distortions and we can use it to identify recent merger systems that are highly distorted. In previous studies a galaxy was taken to be a recent merger if its asymmetry index is $A > A_m$, with $A_m = 0.35$ (e.g., Conselice 2003; De Propriis et al. 2007; Bridge et al. 2007). This methodology presents several systematic effects, such as signal-to-noise dependence (Conselice 2003; Conselice et al. 2005), contamination by non-interacting galaxies with high asymmetry values (Jogee et al. 2009; Miller et al.

2008), contamination by nearby bright sources (De Propriis et al. 2007), or the pass-band in which we measure the asymmetry (Cassata et al. 2005; Taylor-Mager et al. 2007; Conselice et al. 2008), which must be carefully treated to avoid biased merger fractions. In the following sections we detail how we determined the asymmetry index and its dependence on several factors, such as the background image B_0 that we use (Sect. 3.1.1), the pass-band in which we calculate it (Sects. 3.1.2, 3.1.3) and the signal-to-noise of the source (Sects. 3.1.4, 3.2, 3.3).

3.1. Asymmetry calculation

3.1.1. Background dependence

In Eq. (1) we have a dependence on the background image B_0 ; that is, different background images yield different asymmetries for the same source (Conselice et al. 2003). To minimize this effect we determined the asymmetry of each source with five different background images. These background images are sky source-free sections of 50×50 pixels located in the same position in the four HST/ACS filter images, and were chosen to span all the GOODS-S area. The asymmetry of one source was the median of those five background-dependent asymmetries.

3.1.2. Pass-bands and redshift range

Galaxy morphology depends on the band of observation (e.g. Kuchinski et al. 2000; Lauger et al. 2005; Taylor-Mager et al. 2007). In particular, when galaxies contain both old and young populations, morphologies may change very significantly on both sides of the Balmer/4000Å break. The asymmetry index limit $A_m = 0.35$ was established in the rest-frame B -band (Conselice 2003). When dealing with galaxies over a range of redshifts, in order to avoid systematic passband biases with redshift, one needs to apply a so-called morphological K-correction by performing the asymmetry measurements in a band as close as possible to rest-frame B (e.g., Cassata et al. 2005), or apply statistical corrections for obtaining asymmetries in rest-frame B from asymmetry measurements in rest-frame U (Conselice et al. 2008). Taking advantage of the homogeneous multiband imaging provided by the GOODS survey, we entirely avoid morphological K-correction problems in the present study by performing asymmetry measurements on all GOODS-S B_{435} , V_{606} , i_{775} , and z_{850} images, and using for each source the filter that most closely samples rest-frame B .

To determine the redshift ranges over which rest B -band or U -band dominates the flux in the four observational HST/ACS filters, B_{435} , V_{606} , i_{775} , and z_{850} , we defined the function

$$f_{RF}(z) = \frac{\int_0^\infty P_{ACS}(\lambda/(1+z))P_{RF}(\lambda)d\lambda}{\int_0^\infty P_{RF}(\lambda)d\lambda}, \quad (2)$$

where P_{RF} and P_{ACS} are the transmission curves of the rest-frame reference filter and one HST/ACS filter, respectively. In Fig. 2 we show the function $f_B(z)$ for the four ACS filters (black curves), and $f_U(z)$ for z_{850} (grey curve). On the basis of this figure, B_{435} asymmetries were used for $0 < z \leq 0.15$ sources; V_{606} asymmetries for $0.15 < z \leq 0.55$; i_{775} for $0.55 < z \leq 0.9$; and z_{850} for $0.9 < z \leq 1.3$. Staying within rest-frame B imposed a maximum redshift of $z_{\max} = 1.3$.

Note that, because the ML method used in the merger fraction determination (Sect. 4) takes into account the experimental errors, we had to include in the samples not only the sources with $z_i < z_{\text{up}}$, where z_{up} is the upper redshift in our study, but

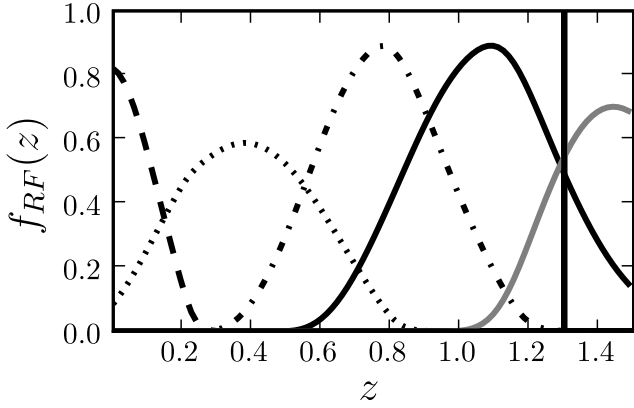


Fig. 2. Function $f_B(z)$ for the four ACS filters: B_{435} (black dashed curve), V_{606} (black dotted curve), i_{775} (black dot-dashed curve), and z_{850} (black solid curve). The grey solid curve is the function $f_U(z)$ for the z_{850} filter. The vertical black solid line is the maximum redshift, $z_{\max} = 1.3$, in our study.

also sources with $z_i - 2\sigma_i < z_{\text{up}}$ in order to ensure completeness. Because of this, z_{up} must fulfil the condition $z_{\max} - 2\sigma_{\delta_z}(1 + z_{\max}) = z_{\text{up}}$, which yields $z_{\text{up}} \sim 1.1$. We took as minimum redshift in our study $z_{\min} = 0.1$ because of the lack of sources at lower redshifts. This yields $z_{\text{down}} = z_{\min} + 2\sigma_{\delta_z}(1 + z_{\min}) \sim 0.2$, which ensures completeness and good statistics. Applying these redshift limits we finally have 1740 galaxies with $M_B \leq -19.5$ and 982 with $M_{\star} \geq 10^{10} M_{\odot}$. The number of galaxies quoted here was obtained after removing problematic border sources (Sect. 3.1.4).

3.1.3. Determining the asymmetry of sources with photometric redshifts

Roughly $\sim 40\%$ of the sources in our samples do not have spectroscopic redshifts and we rely on photometric redshift determinations. In these cases, our source could have its rest-frame B -band flux in two observational ACS filters, within 1σ . To take this into account we assumed three different redshifts for each photometric source: $z_{\text{phot}}^- = z_{\text{phot}} - \sigma_{z_{\text{phot}}}$, z_{phot} , and $z_{\text{phot}}^+ = z_{\text{phot}} + \sigma_{z_{\text{phot}}}$. We determined the asymmetry in these three redshifts. We then performed a weighted average of the three asymmetry values such that:

$$A_0 = 0.16A(z_{\text{phot}}^-) + 0.16A(z_{\text{phot}}^+) + 0.68A(z_{\text{phot}}), \quad (3)$$

where $A(z)$ is the asymmetry of the source at redshift z . We used the same average procedure with the uncertainties of the three asymmetries and added the result in quadrature to the rms of the three asymmetry values to obtain σ_{A_0} . In sources with z_{spec} we only determined the asymmetry at the source redshift. L09 show that the two different asymmetry determinations do not introduce systematic differences between sources with and without spectroscopic information.

3.1.4. Boundary effects and bright source contamination

The signal-to-noise in HST/ACS decreases near the boundaries of the images, where the exposure time is lower. This affects our asymmetry values in two ways: the SExtractor segmentation maps that we use to calculate the asymmetry have many spurious detections, and any of the five backgrounds defined in

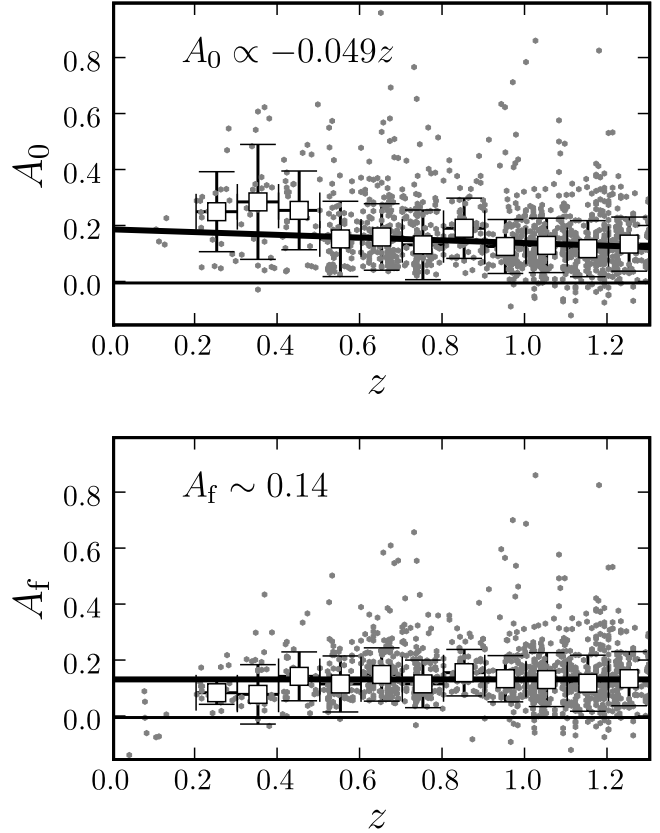


Fig. 3. Asymmetry vs redshift in the $M_B \leq -20$ sample (grey dots in both panels). *Top*: asymmetries of the sources measured on the original images. *Bottom*: asymmetries of the sources measured on images artificially redshifted to $z_d = 0.1$. Open squares in both panels are the mean asymmetries in 0.1 redshift bins. The black solid line is the least-squares linear fit to the mean asymmetries in the $[0.5, 1.3]$ redshift interval.

Sect. 3.1.1 is representative of the noisier source background. The problem with segmentation maps was noticed previously by De Propriis et al. (2007), where the segmentation maps for 50% of their initial 129 galaxies with $A > 0.35$ are incorrect, or are contaminated by bright nearby sources. With this in mind, we visually inspected all the sources looking for boundary or contaminated sources. We found that boundary sources had systematically high asymmetry values, and had segmentation maps contaminated by spurious detections. To avoid biased merger fraction values we excluded all border sources (high and low asymmetric) from the samples. We found only two sources contaminated by bright nearby sources. For these we redefined the SExtractor parameters to construct correct segmentation maps and redetermined the asymmetry.

3.2. Asymmetries at a Reference Redshift

The asymmetry index measured on survey images systematically varies with the source redshift due, first, to the $(1+z)^4$ cosmological surface brightness dimming, which can modify the galaxy area over which asymmetry is measured, and, second, to the loss of spatial resolution with z . Several papers have attempted to quantify these effects by degrading the image spatial resolution and flux to simulate the appearance that a given galaxy would have at different redshifts in a given survey. Conselice et al.

(2003, 2008); and Cassata et al. (2005) degraded a few local galaxies to higher redshifts and found that asymmetries decrease with z . Conselice et al. (2003) also noted that this decrease depends on image depth, and that luminous galaxies are less affected. In addition, Conselice et al. (2005) show that irregular (high asymmetry) galaxies are more affected than ellipticals (low asymmetry). A zeroth-order correction for such biases was implemented by Conselice et al. (2003, 2008, 2009) who applied a ΔA_z term, defined as the difference between the asymmetry of local galaxies measured in the original images and the asymmetry of the same galaxies in the images degraded to redshift z . Their final, corrected asymmetries are $A_f = A_0 + \Delta A_z$, where A_0 is the asymmetry measured in the original images. With these corrections, all the galaxies have their asymmetry referred to $z = 0$, and the local merger criterion $A > A_m = 0.35$ is then used.

In their study, L09 improve on the above procedure, and we apply their methodology to our data set. We compute a correction term individually for each source in the catalogue, but rather than attempting to recover $z = 0$ values for A we degrade each of the galaxy images to redshift $z_d = 1$; we then obtain our final asymmetry values A_f directly from the degraded images. With this procedure, we take into account that each galaxy is affected differently by the degradation; e.g. the asymmetry of a low luminosity irregular galaxy dramatically decreases with redshift, while a luminous elliptical is slightly affected. We choose $z_d = 1$ as our reference redshift because a source at this (photometric) redshift has $z_d + \sigma_{z_d} \sim z_{\text{up}} = 1.1$; that is, the probability that our galaxy belongs to the range of interest is $\sim 85\%$. Because we work with asymmetries reduced to $z_d = 1$, the asymmetry criterion for mergers, A_m , needs to be reduced to $z = 1$. We discuss this in Sect. 3.3.

We have already mentioned that $\sim 60\%$ of the sources in the samples have spectroscopic redshifts, hence redshift information coming from photometric redshifts for the remaining $\sim 40\%$ of the sources has large uncertainties. As in the A_0 calculation process (Sect. 3.1.3, Eq. [3]), to take into account the redshift uncertainty when deriving the asymmetries at $z_d = 1$ we started from three different initial redshifts for each source, $z_{\text{phot}}^- = z_{\text{phot}} - \sigma_{z_{\text{phot}}}$, z_{phot}^+ , and z_{phot} , and degraded the image from these three redshifts to $z_d = 1$. We then performed a weighted average of the three asymmetry values such that

$$A_f = 0.16A_1(z_{\text{phot}}^-) + 0.16A_1(z_{\text{phot}}^+) + 0.68A_1(z_{\text{phot}}), \quad (4)$$

where $A_1(z)$ denotes the asymmetry measured in the image degraded from z to $z_d = 1$. When a spectroscopic redshift was available, the final asymmetry was simply $A_f = A_1(z_{\text{spec}})$. We did not apply any degradation to sources with $z > 1$; that is, we assumed that $A_1(z > 1) = A_0$.

To obtain the error of the asymmetry, denoted by σ_{A_f} , for sources with photometric redshifts, we averaged the uncertainties of the three asymmetries following Eq. (4) and added the result in quadrature to the rms of the three asymmetry values. The first term accounts for the signal-to-noise error in the asymmetry value, while the second term is only important when differences between the three asymmetry values cannot be explained by the signal-to-noise first term. In sources with spectroscopic redshifts we took as σ_{A_f} the uncertainty of the asymmetry $A_1(z_{\text{spec}})$.

The degradation of the images was performed with `COSMOSHIFT` (Balcells et al. 2003), which performs repixelation, psf change and flux decrease over the sky-subtracted source image. The last `COSMOSHIFT` step is the addition of a random Poisson sky noise to the degraded source image to mimic the noise level of

Table 1. Degradation rate for different luminosity samples

Sample selection	n_{tot} (1)	δ_A (2)	A_0 (3)
$M_B \leq -19.5$	1740	-0.09 ± 0.01	0.156
$M_B \leq -19.75$	1402	-0.07 ± 0.01	0.160
$M_B \leq -20$	1122	-0.05 ± 0.01	0.163
$M_B \leq -20.25$	869	-0.05 ± 0.02	0.165
$M_B \leq -20.5$	648	-0.04 ± 0.02	0.161

NOTES. Col. (1) Number of sources in the sample with $0.1 \leq z < 1.3$. Col. (2) Degradation rate of the asymmetry, $\Delta A = \delta_A \Delta z$. Col. (3) Median asymmetry of sources with $z < 1$.

the data. As a result of this last step, two `COSMOSHIFT` degradations of the same source yield different asymmetry values. We took the asymmetry of each degraded source, $A_1(z)$, to be the median of asymmetry measurements on five independent degradations of the original source image from z to $z_d = 1$. With all the aforementioned steps, each $A_1(z)$ determination involved 25 asymmetry calculations, while the uncertainty in $A_1(z)$ was the median of the five individual asymmetry errors.

The asymmetries A_f referred to $z_d = 1$ provide a homogeneous asymmetry set that permits consistent morphological studies in the GOODS-S field (López-Sanjuan et al. 2009b, in preparation).

3.3. Asymmetry Trends with Redshift

For a sample of galaxies over a range of redshifts, the statistical change with z of the measured asymmetries A_0 is the combined effect of loss of information (as shown in the previous section) and changes in the galaxy population. In contrast, the redshift evolution of A_f reflects changes in the galaxy population alone, given that the morphological information in the images used to determine A_f is homogeneous for the sample. As already discussed in L09 for the Groth field, we show here that the z trends of A_0 and A_f are quite different.

In the top panel of Fig. 3 we show the variation of A_0 with redshift in a $M_B \leq -20$ selected sample, while in the bottom panel we see the variation of A_f for the same sample. In both panels, open squares are the median asymmetries in $\Delta(z) = 0.1$ redshift bins, and the black solid line is the best linear least-squares fit to the $0.5 \leq z < 1.3$ points. A_0 is seen to decrease with redshift, $A_0 = 0.19 - 0.049z$, while the A_f distribution is flat, $A_f \sim 0.14$. For A_0 , the negative slope reflects the fact that the loss of information with redshift (negative effect on A) dominates over genuine population variations (a positive effect because galaxies at higher redshift are more asymmetric; e.g. Cassata et al. 2005; Conselice et al. 2005). In A_f the information level does not vary with the redshift of the source, so we only see population effects. In this case the slope is null, but this is a field-to-field effect: L09, with the same methodology and sample selection, obtain $A_f \propto 0.05z$. This indicates that we cannot extrapolate results from one field to another, and that individual studies of systematics are needed. We take as degradation rate (δ_A) the difference between both slopes and assume that the merger condition A_m varies with redshift as $A_m(z) = A_m(0) - \delta_A z = 0.35 - \delta_A z$.

Is the degradation rate the same for all luminosity selections? We expect less asymmetry variation with redshift in bright samples, because they are less affected by cosmological dimming (Conselice 2003). We repeated the previous analysis with different M_B selection cuts, from $M_B \leq -20.5$ to $M_B \leq -19.5$

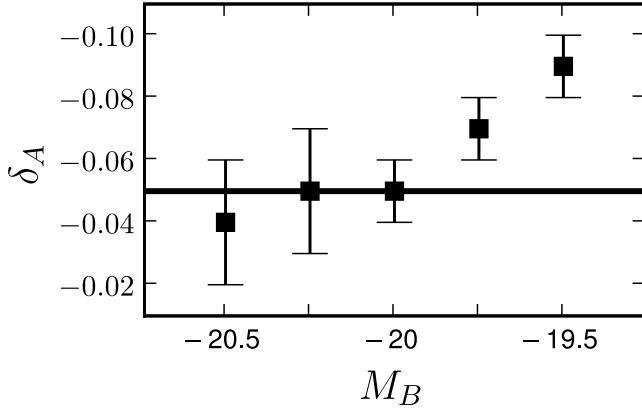


Fig. 4. Degradation rate δ_A vs the selection magnitude M_B of the sample (black squares). The black solid line marks $\delta_A = -0.05$, the estimated degradation rate for $M_B \leq -20$ galaxies.

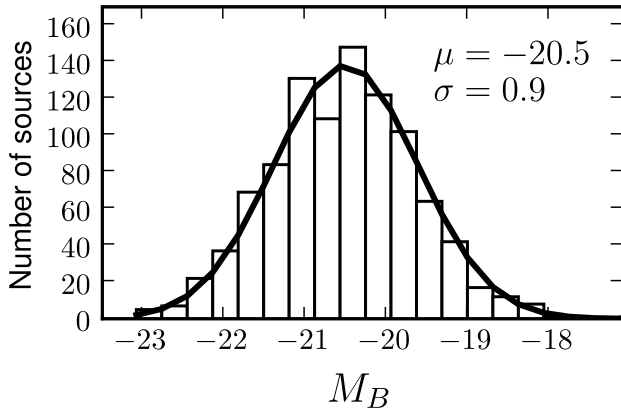


Fig. 5. M_B distribution of $M_* \geq 10^{10} M_\odot$ galaxies. The black solid line is a Gaussian with $\mu = -20.5$ and $\sigma = 0.9$.

(the latter is the limiting magnitude in our study, Sect. 2.2). We summarize the results in Table 1 and Fig. 4: asymmetry is more affected by redshift changes in less luminous samples, as expected. Interestingly, the degradation rate is roughly constant up to $M_B = -20$, $\delta_A \sim -0.05$ (black solid line in Fig. 4), but then becomes more pronounced by a factor of 2, $\delta_A \sim -0.09$, in only 0.5 magnitudes. One could argue that the sharp increase of δ_A for samples including $M_B > -20$ sources arises because such sources have higher initial asymmetry A_0 : a faint irregular galaxy is more affected by loss of information than a bright elliptical. However, we see in the last column of Table 1 that the mean asymmetry of sources with $z < 1.0$ is similar in all samples, $\bar{A}_0 \sim 0.16$. Hence, the degradation rate increases because faint sources have lower signal-to-noise than luminous ones. Because of this, we decided to restrict our study to the 1122 sources with $M_B \leq -20$ to ensure that degradation affects all the galaxies in our sample in the same way, making the merger condition $A_m(1) = 0.35 - \delta_A = 0.30$ representative.

How important is this luminosity dependence for the mass-selected sample? The M_B distribution of $M_* \geq 10^{10} M_\odot$ galaxies is well described by a Gaussian with $\mu = -20.5$ and $\sigma = 0.9$, Fig. 5. We found that 70% of the galaxies have $M_B \leq -20$, and that the degradation rate for the whole sample is $\delta_A = -0.05$. This tells us that the faint sources in this sample do not significantly affect the degradation rate, making the $M_B \leq -20$ merger

condition representative also for the mass-selected sample. In conclusion, we used $A_m(1) = 0.30$ for both samples.

4. MERGER FRACTION DETERMINATION

Following Conselice (2006b), the merger fraction by morphological criteria is

$$f^{\text{mph}} = \frac{\kappa \cdot n_m}{n_{\text{tot}} + (\kappa - 1)n_m}, \quad (5)$$

where n_m is the number of the distorted sources with $A > A_m$, and n_{tot} is the total number of sources in the sample. If $\kappa \geq 2$ we obtain the galaxy merger fraction, $f_{\text{gm}}^{\text{mph}}$, the fraction of galaxies undergoing mergers, and κ represents the average number of galaxies that merged to produce one distorted remnant. If $\kappa = 1$ we obtain the merger fraction, f_m^{mph} : the number of merger events in the sample. We use $\kappa = 1$ throughout this paper.

The steps we followed to obtain the merger fraction are described in detail in LGB08. In this section we provide a short summary. If we define a two-dimensional histogram in the redshift–asymmetry space and normalize this histogram to unity, we obtain a two-dimensional probability distribution defined by the probability of having one source in the bin $[z_k, z_{k+1}) \cap [A_l, A_{l+1})$, namely p_{kl} , where the index k spans the redshift bins of size Δz , and the index l spans the asymmetry bins of size ΔA . We consider only two asymmetry bins split at A_m , such that the probabilities p_{k1} describe highly distorted galaxies (i.e. merger systems), while the probabilities p_{k0} describe normal galaxies. With those definitions, the morphologically based merger fraction in the redshift interval $[z_k, z_{k+1})$ becomes

$$f_{m,k}^{\text{mph}} = \frac{p_{k1}}{p_{k0} + p_{k1}}. \quad (6)$$

In LGB08 they describe a maximum likelihood (ML) method that yields the most probable values of p_{kl} taking into account not only the z and A values, but also their experimental errors. The method is based on the minimization of the joint likelihood function, which in our case is

$$L(z_i, A_i | p'_{kl}, \sigma_{z_i}, \sigma_{A_i}) = \sum_i \left[\ln \left\{ \sum_k \sum_l \frac{e^{p'_{kl}}}{4} \text{ERF}(z, i, k) \text{ERF}(A, i, l) \right\} \right], \quad (7)$$

where

$$\text{ERF}(\eta, i, k) \equiv \text{erf} \left(\frac{\eta_i - \eta_{k+1}}{\sqrt{2}\sigma_{\eta_i}} \right) - \text{erf} \left(\frac{\eta_i - \eta_k}{\sqrt{2}\sigma_{\eta_i}} \right). \quad (8)$$

In the above equations, $\text{erf}(x)$ is the error function; z_i and A_i are the redshift and asymmetry values of source i , respectively; σ_{z_i} and σ_{A_i} are the observational errors in redshift and asymmetry of source i , respectively; and the new variables $p'_{kl} \equiv \ln(p_{kl})$ are chosen to avoid negative probabilities. Equation (7) was obtained by assuming that the real distribution of galaxies in the redshift–asymmetry space is described by a two-dimensional distribution $p_{kl} \equiv \exp(p'_{kl})$, and that the experimental errors are Gaussian. Note that changing variables to $p'_{kl} = \ln(p_{kl})$, Eq. (6) becomes

$$f_{m,k}^{\text{mph}} = \frac{e^{p'_{k1}}}{e^{p'_{k0}} + e^{p'_{k1}}}. \quad (9)$$

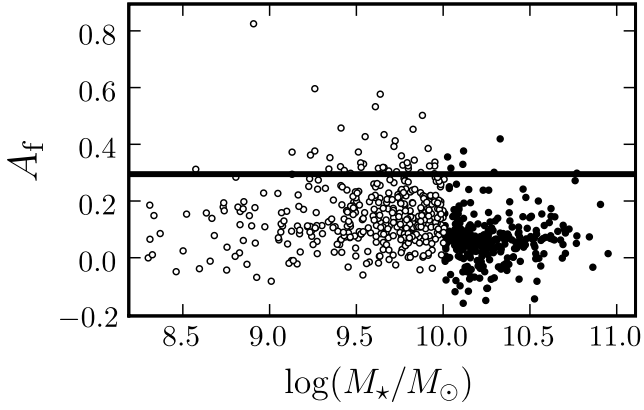


Fig. 6. Asymmetry vs $\log(M_*/M_\odot)$ for *light-weight* (open circles) and *faint* (bullets) samples (see text for details). The black solid line shows the merger criterion $A_m(1) = 0.30$.

LGB08 show, using synthetic catalogues, that the experimental errors tend to smooth an initial two-dimensional distribution described by p_{kl} , due to spill-over of sources to neighbouring bins. This leads to a $\sim 10 - 30\%$ overestimate of the galaxy merger fraction in typical observational cases. L09 and Lotz et al. (2008a) find similar trends in their study of the morphological merger fraction in the Groth Strip. LGB08 additionally show that, thanks to the use of the ML method, they can accurately recover the initial two-dimensional distribution: the fractional difference between the input and ML method merger fractions is a tiny $\sim 1\%$ even when the experimental errors are similar to the bin size. That is, the ML results are not biased by the spill-over of sources to neighbouring bins.

We obtained the morphological merger fraction by applying Eq. (9) using the probabilities p'_{kl} recovered by the ML method. In addition, the ML method provides an estimate of the 68% confidence intervals of the probabilities p'_{kl} , which we use to obtain the $f_{m,k}^{\text{mph}}$ 68% confidence interval, denoted $[\sigma_{f_{m,k}^{\text{mph}}}^-, \sigma_{f_{m,k}^{\text{mph}}}^+]$.

This interval is asymmetric because $f_{m,k}^{\text{mph}}$ is described by a log-normal distribution due to the calculation process (see LGB08 for details). Note that, in LGB08, $\kappa = 2$ is used in Eq. (5), but the method is valid for any κ value.

We also determined the morphological merger fraction by classical counts, $f_{m,\text{class}}^{\text{mph}} = n_m^{\text{class}}/n_{\text{tot}}^{\text{class}}$, where n_m^{class} is the number of galaxies in a given bin with $A_f > A$, and $n_{\text{tot}}^{\text{class}}$ is the total number of sources in the same bin. We obtained the $f_{m,\text{class}}^{\text{mph}}$ uncertainties assuming Poissonian errors in the variables.

Finally, and following L09, sect. 4.1, we performed simulations with synthetic catalogues to determine the optimum binning in redshift for which the ML method results are reliable. The simulations were made in the same way as in L09, so here we only report the results of the study: we can define up to three redshift bins, namely $z_1 = [0.2, 0.6)$, $z_2 = [0.6, 0.85)$, and $z_3 = [0.85, 1.1)$. The first bin is wider than the other two, 0.4 vs 0.25, because of the lower number of sources in the first interval. In the next section we study the merger fraction evolution with redshift with these three bins (§ 5.1). We will also provide statistics for the $z_0 = [0.2, 1.1)$ bin in order to compare the ML and classical merger fraction determinations.

5. RESULTS

We summarize in Table 2 the main characteristics of the two samples under study; i.e. the total (n_{tot}) and distorted (n_m) number of sources, both for classical counts (n^{class}) and the ML method (n^{ML}), and major merger fractions. Note that the number of ML method galaxies is not an integer. Indeed, the ML method gives us a statistical estimate of the probability $p_{kl} = \exp(p'_{kl})$ of finding one source in the redshift bin k , and in the asymmetry bin l , so the estimated number of galaxies in that bin, $n_{kl,\text{ML}} = N_{\text{tot}} p_{kl} \Delta z \Delta A$, where N_{tot} is the total number of galaxies in the sample, need not be an integer. The merger fraction by the ML method is roughly half that in the classical determination (0.035 vs 0.077 in the luminosity-selected sample, 0.025 vs 0.050 in the mass-selected sample). This highlights the fact that, whenever the spill-over effect of large measurement errors is not taken into account, morphological merger fractions can be overestimated by a factor of ~ 2 . We use this result later in Sect. 6.3, and in the next section we use only merger fractions obtained by the ML method.

We find that correction of redshift-dependent biases is equally important. If we use the raw asymmetry values determined on the original images, and apply the local Universe merger selection criterion $A_0 > 0.35$, the resulting merger fractions come up a factor 2 higher than the ones listed in Table 2. Recall that the latter come from A_f values homogenised to a common reference $z_d = 1$ (Sect. 3.2). This emphasises that published merger fractions which do not work with redshift-homogeneous data, may be significantly biased. Interestingly, an identical comparison to the one just described, applied to Groth strip data, lead L09 to conclude that redshift effects are *not* important for merger fraction determinations. The different behaviour of the Groth data from L09 and our GOODS-S data might be due to cosmic variance, or to depth differences between the two data sets. In general though, artificial redshifting of the galaxies is needed to ensure reliable results.

Table 2 shows that the merger fraction from the mass-selected sample is lower than that from the luminosity-selected sample. What is the origin of this difference? To answer this question, we define two subsamples: the *faint* sample (galaxies with $M_B > -20$ and $M_* \geq 10^{10} M_\odot$), and the *light-weight* sample (sources with $M_* < 10^{10} M_\odot$ and $M_B \leq -20$). The *faint* sample comprises 272 sources, while the *light-weight* sample comprises 408 sources. In Fig. 6 we show both samples in the mass–asymmetry plane: light-weight galaxies have higher asymmetry, $\bar{A}_f = 0.14$, while faint galaxies are more symmetric, $\bar{A}_f = 0.07$. The *light-weight* sample comprises 43 sources with $A_f > 0.30$ (10.5% of the sample), while the *faint* sample comprises only seven distorted sources (2.5% of the sample). These numbers suggest, in agreement with L09, that: (i) an important fraction of the *B*-band high asymmetric sources are low-mass disc–disc merger systems that, due to merger-triggered star-formation, have their *B*-band luminosity boosted by 1.5 magnitudes (Bekki & Shioya 2001), enough to fulfil our selection cut $M_B \leq -20$; and (ii) the faint objects are earlier types dominated by a spheroidal component which, when subject to a major merger, does not distort enough to be picked up as merger systems by our asymmetry criterion.

5.1. Merger fraction evolution

We summarize in Table 3 the morphological merger fraction at different redshifts in GOODS-S. We obtain low merger fractions, always lower than 0.06, similar to the L09 results for the Groth

Table 2. Sample characteristics in the $0.2 \leq z < 1.1$ range

Sample selection	$n_{\text{tot}}^{\text{class}}$ (1)	$n_{\text{m}}^{\text{class}}$ (2)	$f_{\text{m,class}}^{\text{mph}}$ (3)	$n_{\text{tot}}^{\text{ML}}$ (4)	n_{m}^{ML} (5)	$f_{\text{m,ML}}^{\text{mph}}$ (6)
$M_B \leq -20$	793	61	0.077 ± 0.010	881.9	30.7	$0.035^{+0.010}_{-0.008}$
$M_{\star} \geq 10^{10} M_{\odot}$	759	38	0.050 ± 0.008	819.3	20.2	$0.025^{+0.008}_{-0.006}$

NOTES. Col. (1) Number of galaxies with $0.2 \leq z < 1.1$ by classical counts. Col. (2) Number of distorted galaxies with $0.2 \leq z < 1.1$ and $A_f > 0.30$ by classical counts. Col. (3) Morphological major merger fraction by classical counts. Col. (4) Number of galaxies with $0.2 \leq z < 1.1$ by ML method. Col. (5) Number of distorted galaxies with $0.2 \leq z < 1.1$ and $A_f > 0.30$ by ML method. Col. (6) Morphological major merger fraction by ML method.

Table 3. Morphological major merger fractions $f_{\text{m}}^{\text{mph}}$ in GOODS-S

Sample selection	$z = 0.4$	$z = 0.725$	$z = 0.975$	$f_{\text{m}}^{\text{mph}}(0)^{\text{a}}$	m^{a}
$M_B \leq -20$	$0.023^{+0.022}_{-0.011}$	$0.031^{+0.016}_{-0.011}$	$0.043^{+0.015}_{-0.011}$	$0.013 \pm 0.003^{\text{b}}$	$1.8 \pm 0.5^{\text{b}}$
$M_{\star} \geq 10^{10} M_{\odot}$	$0.006^{+0.018}_{-0.005}$	$0.022^{+0.013}_{-0.008}$	$0.037^{+0.016}_{-0.011}$	$(1.0 \pm 0.2) \times 10^{-3}$	5.4 ± 0.4

^a Best $f_{\text{m}}^{\text{mph}}(z) = f_{\text{m}}^{\text{mph}}(0)(1+z)^m$ fit to the data.

^b This fit includes the De Propris et al. (2007) local value.

Table 4. Morphological merger fraction in GOODS-S at $0.6 \leq z < 0.85$

Sample selection	n_{LSS} (1)	w/ LSS (2)	w/o LSS (3)	LSS ($z = 0.735$) (4)
$M_B \leq -20$	72	$0.031^{+0.016}_{-0.011}$	$0.026^{+0.020}_{-0.011}$	$0.044^{+0.032}_{-0.018}$
$M_{\star} \geq 10^{10} M_{\odot}$	94	$0.022^{+0.013}_{-0.008}$	$0.018^{+0.016}_{-0.008}$	$0.032^{+0.023}_{-0.014}$

NOTES. Col. (1) Number of galaxies in the Large Scale Structure (LSS). Col. (2) Merger fraction in the sample *with* LSS. Col. (3) Merger fraction in the sample *without* LSS. Col. (4) Merger fraction in the LSS.

field. The merger fraction increases with redshift in both the luminosity- and the mass-selected samples, but this growth is more prominent in the mass-selected sample. We can parameterize the merger fraction evolution as

$$f_{\text{m}}^{\text{mph}}(z) = f_{\text{m}}^{\text{mph}}(0)(1+z)^m \quad (10)$$

and fit our data. Note that, in the luminosity-selected sample, we also use the $M_B \leq -20$ estimation from L09 of the $M_B \leq -19$ local merger fraction, drawn from the MGC² (Millenium Galaxy Catalogue), from De Propris et al. (2007): $f_{\text{m}}^{\text{mph}}(0.07) = 0.014^{+0.003}_{-0.003}$. We summarize the results in Table 3 and Fig. 7. The merger index m is higher (3σ) in the mass-selected sample (bullets) than in the luminosity-selected sample (open triangle for De Propris et al. 2007 local value; open squares for our data), 5.4 vs 1.8, while the merger fraction in the local universe is lower in the mass-selected sample, 0.001 vs 0.013. The fact that the higher m , the lower $f_{\text{m}}^{\text{mph}}(0)$, was predicted by semianalytical models (Khochfar & Burkert 2001). We compare these values with those from previous studies in Sect. 6.2.

5.2. Large Scale Structure effect

It is well known that the more prominent large scale structure (LSS) in the GOODS-S field is located at redshift $z = 0.735$ (Ravikumar et al. 2007). In order to check the effect of this LSS

on our derived merger fractions, we recalculated them by excluding the sources within $\delta v \leq 1500 \text{ km s}^{-1}$ ($\delta z \sim 0.01$) of $z = 0.735$ (Rawat et al. 2008). In Table 4 we summarize the number of sources in the LSS for each sample (n_{LSS}), and the previous and recalculated merger fractions, both in the field and in the structure. The merger fraction is higher in the LSS than in the field. Note that the variation in the field values is well reported by the error bars. How does this LSS affect the previously inferred merger evolution? If we again fit the data without LSS, we find that $f_{\text{m}}^{\text{mph}}(0)$ does not change, while the value of m decreases only by 0.1 in both the luminosity- and the mass-selected samples, so our conclusions remain the same. We shall therefore use the fit values in Table 3 in the remainder of the paper. We concentrate on the LSS at $z = 0.735$, and ignore other structures in GOODS-S. The next two more important ones are located at $z = 0.66$ and $z = 1.1$. The former is an overdensity in redshift space, but not in the sky plane, while the latter is a cluster, but comprises an order of magnitude fewer sources than the $z = 0.735$ structure (145 vs 12, Adami et al. 2005).

6. DISCUSSION

First we compare our results with merger fraction determinations from other authors. In Fig. 7 we show our results (open squares for $M_B \leq -20$ galaxies and bullets for $M_{\star} \geq 10^{10} M_{\odot}$ galaxies). The other points are those from the literature: the $M_B \leq -20$ estimate by L09 of the De Propris et al. (2007) $M_B \leq -19$ merger fraction; the merger fraction for B -band luminosity

² www.eso.org/~jliske/mgc

selected galaxies in AEGIS³ (All-Wavelength Extended Groth Strip International Survey) from Lotz et al. (2008a); the results from Conselice et al. (2009) in COSMOS⁴ (Cosmological Evolution Survey) and AEGIS for $M_\star \geq 10^{10} M_\odot$ galaxies; and the merger fraction for $M_\star \geq 5 \times 10^{10} M_\odot$ galaxies in GEMS⁵ (Galaxy Evolution from Morphology and SEDs) from Jogee et al. (2009). Note that the mass selection from Jogee et al. (2009) has been adapted to a Salpeter IMF (Salpeter 1955). All the previous merger fractions except those from Jogee et al. (2009) are from automatic indices for major mergers. The Jogee et al. (2009) results are by visual morphology and reflect major+minor mergers; the dashed rectangle marks their expected major merger fraction. For luminosity-selected samples (open symbols) our values are in good agreement with De Propriis et al. (2007), but are lower than those from Lotz et al. (2008a), who apply different sample selection and merger criteria from ours and do not correct the effect of observational errors, thus making comparison difficult.

In the mass-selected case our results are in good agreement with the expected visual major merger fraction from Jogee et al. (2009) (dashed lines), supporting the robustness of our methodology for obtaining major merger fractions statistically. Our values are significantly lower than those of Conselice et al. (2009), especially at $z \gtrsim 0.7$, where there is a factor 3 difference. The asymmetry calculation performed by Conselice et al. (2009) does not take into account the spill-over effect of observational errors in their merger fraction determination. We show here that such effects may lead to the higher value obtained by them. Conselice et al. (2009) assume two main statistical corrections at $z \gtrsim 0.7$: the information degradation bias (ΔA_z , § 3.2) and the morphological K-correction (ΔA_K , see Conselice et al. 2008, for details). The first correction is $\Delta A_z = 0.5$ and has an associated uncertainty of $\sigma_{\Delta A_z} \sim 0.08$ (Conselice et al. 2003, Table 1). The morphological K-correction depends on redshift; to simplify the argument, we do not consider its uncertainty in the following. In addition, each source asymmetry has its own signal-to-noise uncertainty, which in our study is ~ 0.03 at these redshifts. We reproduced the same methodology applied by Conselice et al. (2009) on synthetic catalogs created as in Sect. 4. For further details about simulation parameters and assumptions, see L09. In the simulations we defined two redshift intervals, namely $z_2 = [0.6, 0.85]$ and $z_3 = [0.85, 1.1]$, taking our results in these redshift intervals as input merger fractions, $f_m^{\text{mph}} = 0.022$ in the first interval, and $f_m^{\text{mph}} = 0.037$ in the second. We then extracted 2000 random sources in the redshift-asymmetry plane, applying an asymmetry error to them of $\sigma_A = 0.08$, which is representative of the asymmetry uncertainties in Conselice et al. (2009). We assumed $\sigma_z = 0$ for simplicity. Merger fractions were derived from classical histograms as in Conselice et al. (2009). We repeated this process 100 times and averaged the results. This process yields $f_m^{\text{mph}} \sim 0.11$ in the first interval, and $f_m^{\text{mph}} \sim 0.13$ in the second, which is similar to Conselice et al. (2009) results at these redshifts. In contrast, the ML method was able to recover the input merger fractions. The exercise demonstrates that the observed differences between the two studies can be naturally explained as a bias introduced in Conselice et al. (2009) by not accounting for spill-over of sources due to observational errors. The fact that Conselice et al. (2009) study is performed over ~ 20000 galaxies, 20 times more sources than in our study,

cannot correct the errors. As emphasized by LGB08, experimental systematic errors are not cured by increasing sample size: the ML method is needed.

6.1. Groth vs GOODS-S merger fractions: cosmic variance effect

L09 report a morphological merger fraction

$$f_{m,\text{GS}}^{\text{mph}}(z = 0.6, M_B \leq -20) = 0.045_{-0.011}^{+0.014} \quad (11)$$

in the Groth field (open diamond in Fig. 7). How does this value compare with the one obtained in GOODS-S? If we use the same selection as in L09, this is, $M_B \leq -20$ galaxies with $0.35 \leq z < 0.85$, the major merger fraction in GOODS-S is

$$f_{m,\text{GOODS}}^{\text{mph}}(z = 0.6, M_B \leq -20) = 0.032_{-0.009}^{+0.013} \quad (12)$$

We can see that both values are consistent within their errors. Because both values are determined using the same methodology and sample selection, the difference of $\Delta f_m = 0.013$ may be explained by cosmic variance, denoted by σ_v . Following Somerville et al. (2004), we infer that the effect of cosmic variance for the typical merger density ($\sim 10^{-4} \text{ Mpc}^{-3}$, Sect. 6.4) and GOODS-S/Groth volume is $\sim 60\%$. That is, we expect $\sigma_v \sim 0.027$ in Groth and $\sigma_v \sim 0.019$ in GOODS-S, so the difference between both merger fraction determinations can indeed be explained as cosmic variance effect. Averaging both values, the morphological merger fraction at $z = 0.6$ is

$$f_m^{\text{mph}}(z = 0.6, M_B \leq -20) = 0.038 \pm 0.012, \quad (13)$$

where the error is the expected $\sigma_v \sim 30\%$ due to combining two separate fields (see Somerville et al. 2004, for details).

6.2. Morphological merger fraction evolution in previous studies

In Sect. 5.1 we obtained the values of m and $f_m^{\text{mph}}(0)$ that describe the morphological merger fraction evolution in GOODS-S. In this section we compare these values with those in the literature, where morphological works in B -band selected samples are common. L09 study the merger fraction for $M_B \leq -20$ galaxies in Groth by asymmetries and taking into account the experimental error bias. Combining their results with the literature, they obtain $m = 2.9 \pm 0.8$, consistent to within $\sim 1\sigma$ with our result. Lotz et al. (2008a) study the merger fraction in an $M_B \leq -18.83 - 1.3z$ selected sample by G and M_{20} morphological indices. Their results alone suggest $m = 0.23 \pm 1.03$, but when combined with others in the literature they obtain $m = 2.09 \pm 0.55$. The first case does not match the local morphological merger fraction by De Propriis et al. (2007): with a similar luminosity cut, $M_B \lesssim -19$, and taking into account the different methodologies (see L09, for details), the merger fractions are very different, 0.006 (De Propriis et al. 2007) vs 0.07 (Lotz et al. 2008a). Because of this, the second m value is preferred. Kampczyk et al. (2007) study the fraction of visually distorted galaxies in SDSS⁶ (Sloan Digital Sky Survey, local value) and COSMOS ($z \sim 0.7$ value) for $M_B \leq -19.15$ galaxies. They find that $m = 3.8 \pm 1.8$, higher than our value, but consistent to within $\sim 1\sigma$. Finally, Conselice et al. (2003) study the morphological merger fraction of $M_B \leq -20$ by asymmetries. However,

³ <http://aegis.ucolick.org/>

⁴ <http://cosmos.astro.caltech.edu/index.html>

⁵ <http://www.mpia.de/GEMS/gems.htm>

⁶ <http://www.sdss.org/>

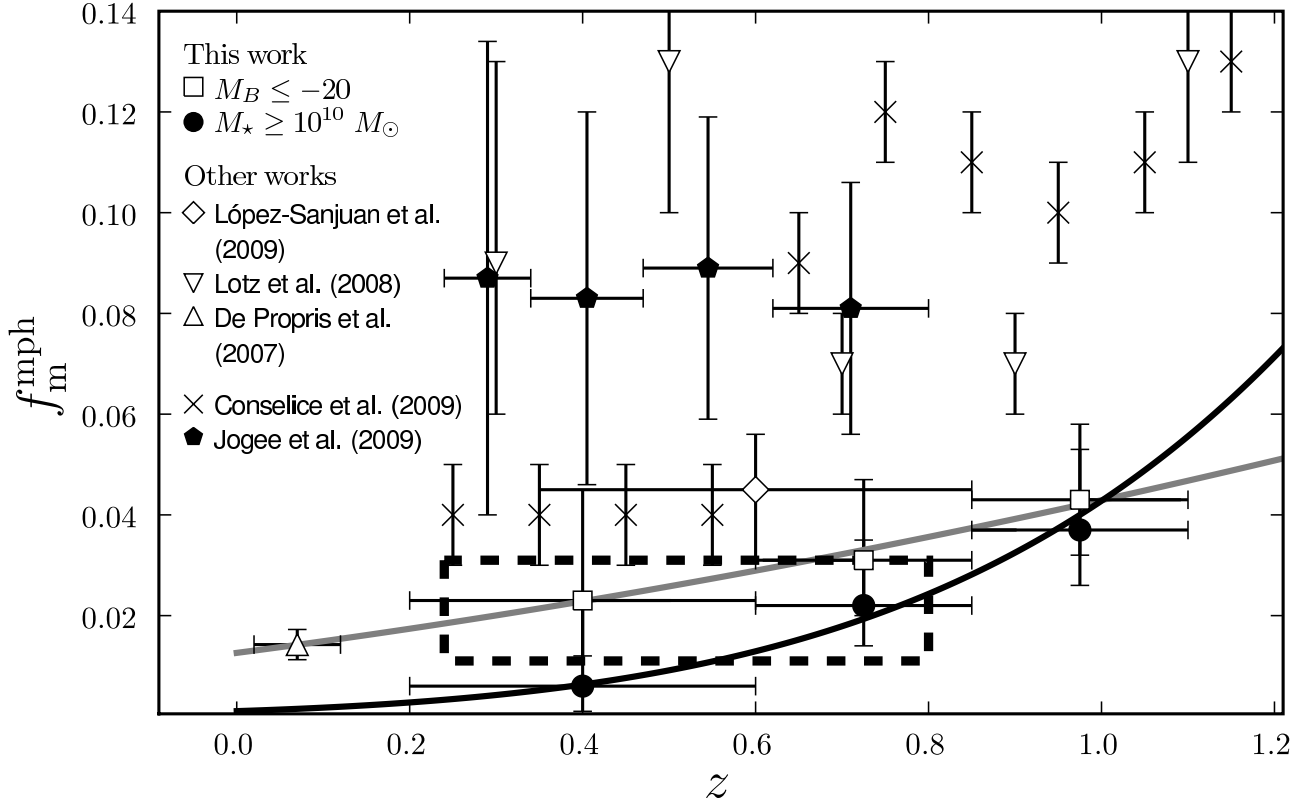


Fig. 7. Morphological merger fraction vs redshift for $M_B \leq -20$ (open squares) and $M_* \geq 10^{10} M_\odot$ galaxies (bullets). The error bars do *not* include cosmic variance (Sec. 6.1). The grey/black solid lines are the least-squares fit of $f_m^{\text{mph}}(z) = f_m^{\text{mph}}(0)(1+z)^m$ to the data in the luminous/mass case, respectively. The open triangle is the $M_B \leq -20$ estimate by L09 of the De Propriis et al. (2007) $M_B \leq -19$ merger fraction, open inverted triangles are from Lotz et al. (2008a), open diamond is for $M_B \leq -20$ galaxies in Groth strip from L09, crosses are for $M_* \geq 10^{10} M_\odot$ galaxies from Conselice et al. (2009), and filled pentagons are minor+major mergers for $M_* \geq 5 \times 10^{10} M_\odot$ galaxies from Jogee et al. (2009). The dashed lines marks the major merger fraction expected by Jogee et al. (2009).

due to the small area of their survey, they have high uncertainties in the merger fraction at $z \lesssim 1$, so we do not compare our results with theirs. In summary, the morphological major merger fraction evolution in M_B samples up to $z \sim 1$ is consistent with a $m = 2.2 \pm 0.4$ evolution (weighted average of the previous m values), although more studies are needed to understand its dependence on different luminosity selections.

The only previous morphological merger fractions in $M_* \geq 10^{10} M_\odot$ selected samples are from Conselice et al. (2003, 2008, 2009). The small areas in the first two studies (HDF⁷ in Conselice et al. 2003 and UDF⁸ in Conselice et al. 2008) make their $z \lesssim 1$ values highly undetermined, and we use their $z \gtrsim 1$ values to constrain the merger fraction evolution at higher redshifts in Sect. 6.3. Conselice et al. (2009) find $m = 3.8 \pm 0.2$. This value is lower than ours, but it is higher than typical values in B -band studies, supporting the hypothesis that merger fraction evolution in mass-selected samples is more important than in luminosity-selected samples.

Other asymmetry studies have used different selection criteria from ours: Cassata et al. (2005) obtain a merger fraction evolution $m = 2.2 \pm 0.3$ in an $m_{K_s} < 20$ selected sample, and combining their results with others in the literature. Bridge et al.

(2007) perform their asymmetry study on a $24\mu\text{m}$ -selected sample ($L_{\text{IR}} \geq 5.0 \times 10^{10} L_\odot$), finding $m = 1.08$. However, these values are difficult to compare with ours because studies with selections in different bands yields different results (Bundy et al. 2004; Rawat et al. 2008; L09).

6.3. Merger fraction evolution at higher redshift

Merger fraction studies of $M_* \geq 10^{10} M_\odot$ galaxies at redshift higher than $z \sim 1$ are rare. Ryan et al. (2008) address the problem with pair statistics, while Conselice et al. (2003, 2008) use asymmetries. Both these studies conclude that the merger fraction shows a maximum at $z \gtrsim 1.5$ and decreases at higher z . This tells us that we cannot extrapolate the power-law fit (Eq. [10]) to high redshift. Fortunately, Conselice et al. (2008) perform their study by asymmetries, providing us with a suitably high redshift reference. Note that, although Conselice et al. (2008) treated the loss of information with redshift, they do not take into account the overestimation due to the experimental errors. Because the Conselice et al. (2008) study is performed in UDF, which is located in the GOODS-S area, we apply a 0.5 factor to the Conselice et al. (2008) merger fractions based on the results of Section 5. In Fig. 8 we show the corrected Conselice et al. (2008) merger fractions (white dots) and our data (black dots). Note that

⁷ <http://www.stsci.edu/ftp/science/hdf/hdf.html>

⁸ <http://www.stsci.edu/hst/udf>

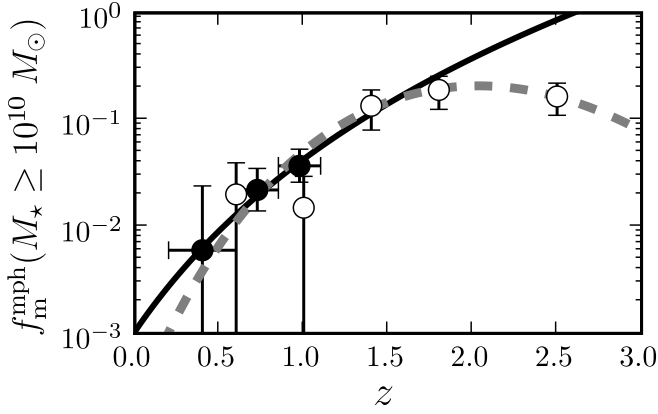


Fig. 8. Morphological merger fraction vs redshift for $M_\star \geq 10^{10} M_\odot$ galaxies. Data are from Conselice et al. (2008, open circles) and this work (bullets). The black solid line gives the least-squares power-law fit to our data, $f_m^{\text{mph}}(z) = 0.001(1+z)^{5.4}$, while the dashed grey line is the least-squares fit to Conselice et al. (2008) data at $z > 1.2$ and ours at $z < 1.2$, $f_m^{\text{mph}}(z) = 0.00034(1+z)^{10.5} e^{-0.57(1+z)^2}$.

the previous power-law fit to our data (black solid line, Sect. 5.1) fails to explain the merger fraction values at $z \gtrsim 1.5$.

Following Conselice (2006b), we parameterize the observed tendency as

$$f_m^{\text{mph}}(z) = \alpha(1+z)^m e^{\beta(1+z)^2}, \quad (14)$$

where the local merger fraction is given by $f_m^{\text{mph}}(0) = \alpha \exp(\beta)$. This form is also obtained for the evolution of the merger rate on the basis of Press–Schechter theory (Carlberg 1990). The best fit of the Conselice et al. (2008) data at $z > 1.2$ and ours at $z < 1.2$ yields $\alpha = 3.4 \times 10^{-4}$, $m = 10.5$, and $\beta = -0.57$ (gray dashed line in Fig. 8). With these values the merger fraction peaks at $z_{\text{peak}} = 2$, in good agreement with Conselice et al. (2008).

The previous parameterization implies that the merger fraction drops at $z > z_{\text{peak}} = 2$, being ~ 0.01 at $z \sim 4$. On the other hand, Hopkins et al. (2008) models suggest that the merger fraction of $M_\star \geq 10^{10} M_\odot$ galaxies still grows at $z > z_{\text{peak}}$, being ~ 0.30 at $z \sim 4$. In fact, the data in Fig. 8 can also be fitted by

$$f_m^{\text{mph}}(z) = \begin{cases} 0.001(1+z)^{5.4} & z < z_c \\ f_{m,c}^{\text{mph}} & z \geq z_c \end{cases}, \quad (15)$$

where $f_{m,c}^{\text{mph}}$ is a constant, and z_c is the redshift in which the merger fraction behaviour changes; that is, when $0.001(1+z_c)^{5.4} = f_{m,c}^{\text{mph}}$. With the two high redshift points in Fig. 8 we estimate that $f_{m,c}^{\text{mph}} \sim 0.18 \pm 0.04$, which yields $z_c = 1.62$. Further studies are needed to constrain the merger fraction evolution at high redshift, but it is clear that the potential approximation is only valid at $z \lesssim 1.5$.

6.4. The major merger rate evolution

We define the major merger rate ($\mathfrak{R}_m^{\text{mph}}$) as the comoving number of major mergers per Gyr within a given redshift interval and luminosity or stellar mass range:

$$\mathfrak{R}_m^{\text{mph}}(z, M) = \rho(z, M) f_m^{\text{mph}}(z, M) T_{m,A}^{-1}, \quad (16)$$

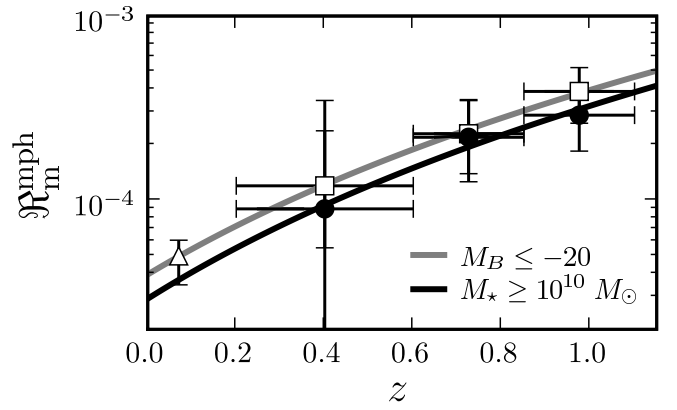


Fig. 9. Morphological merger rate vs redshift for $M_B \leq -20$ (open triangle, De Propriis et al. 2007; open squares, this work) and $M_\star > 10^{10} M_\odot$ galaxies (bullets). The grey/black solid line is the least-squares fit $\mathfrak{R}_m^{\text{mph}}(z) = \mathfrak{R}_m^{\text{mph}}(0)(1+z)^n$ to the data from the luminosity/mass-selected sample, respectively.

where $M = M_B/M_\star$ denotes the selection of the sample, $\rho(z, M)$ is the comoving number density of galaxies at redshift z brighter/more massive than M_B/M_\star , and $T_{m,A}$ is the merger timescale in Gyr for the asymmetry criterion. To obtain $\rho(z, M_B)$ we assume the Faber et al. (2007) luminosity function parameters, while to obtain $n(z, M_\star)$ we assume the Pérez-González et al. (2008) mass function parameters. In addition, we take $T_{m,A} = 0.35 - 0.6$ Gyr. The lower value is from Conselice (2006b, N-body major merger simulations), and the higher from Lotz et al. (2008b, N-body/hydrodynamical equal-mass merger simulations).

We summarize the merger rates in Table 5 and show these values in Fig. 9: white symbols are for $M_B \leq -20$ galaxies (white triangle, De Propriis et al. 2007; white squares, this work) and black dots for $M_\star \geq 10^{10} M_\odot$, while the grey/black solid line is the least-squares fit of $\mathfrak{R}_m^{\text{mph}}(z) = \mathfrak{R}_m^{\text{mph}}(0)(1+z)^n$ function to the data in the luminosity-/mass-selected sample. The parameters of these fits are also summarized in Table 5. In spite of the very different merger fraction evolution, the merger rate evolution of both samples are similar: $n = 3.3 \pm 0.8$ in the luminosity sample, while $n = 3.5 \pm 0.4$ in the mass sample. As in the merger fraction case, the results are not affected by the LSS (Sect. 5.2). The reason why the very different merger fraction evolution tuns into a similar merger rate evolution is the evolution over cosmic time of the number density of galaxies. The number of $M_B \leq -20$ galaxies *decreases* by a factor 3 from $z = 1$ to $z = 0$, while the number of $M_\star \geq 10^{10} M_\odot$ galaxies *increases* by a factor 3 in the same redshift range.

We can compare our inferred merger rate with the post-starburst (PSB) rate reported by Wild et al. (2009). The light of PSB galaxies is dominated by A/F stars. Such galaxies are identifiable by their strong Balmer absorption lines compared to their mean stellar age as measured by their 4000 Å break strength. PSB spectra indicate that the formation of O- and early B-type stars has suddenly ceased in the galaxy. The simulations performed by Johansson et al. (2008) find that the PSB phase can only be reached by disc–disc major merger remnants, so the PSB rate and our merger rate may be similar if an evolutionary path connects both populations. The PSB rate, in the range $0.5 < z < 1$ and for $M_\star \gtrsim 10^{10} M_\odot$ galaxies (Salpeter IMF), is $\mathfrak{R}_{\text{PSB}} = (1.6\text{--}2.9) \times 10^{-4} \text{ Mpc}^{-3} \text{ Gyr}^{-1}$, where the interval re-

Table 5. Major merger rates $\mathfrak{X}_m^{\text{mph}}$ in GOODS-S

Sample selection	$z = 0.4^a$	$z = 0.725^a$	$z = 0.975^a$	$\mathfrak{X}_m(0)^{a,b}$	n^b
$M_B \leq -20$	$1.2^{+1.3}_{-0.6}$	$2.3^{+1.4}_{-0.9}$	$3.9^{+1.9}_{-1.3}$	0.40 ± 0.14^c	3.3 ± 0.8^c
$M_\star \geq 10^{10} M_\odot$	$0.9^{+2.6}_{-0.7}$	$2.2^{+1.5}_{-0.9}$	$2.9^{+1.6}_{-1.0}$	0.29 ± 0.06	3.5 ± 0.4

^a In units of $10^{-4} \text{ Mpc}^{-3} \text{ Gyr}^{-1}$.

^b Best $\mathfrak{X}_m^{\text{mph}}(z) = \mathfrak{X}_m^{\text{mph}}(0)(1+z)^n$ fit to the data.

^c This fit includes the De Propris et al. (2007) local value.

flects the uncertainty in the PSB phase time-scale (0.35–0.6 Gyr, Wild et al. 2009). This value compares well with the inferred disc–disc major merger rate at that range, $\mathfrak{X}_m^{\text{mph}} = (1.2\text{--}3.0) \times 10^{-4} \text{ Mpc}^{-3} \text{ Gyr}^{-1}$. Although the uncertainties in both studies are important, the result suggests that SPB galaxies can be the descendants of our distorted, disc–disc major merger remnants.

6.4.1. Number density of merger remnants

If we integrate the merger rate over cosmic time, we obtain the number density of galaxies that have undergone a disc–disc major merger (ρ_{rem}) in a given redshift range:

$$\rho_{\text{rem}}(z_1, z_2) = \int_{z_1}^{z_2} \mathfrak{X}_m^{\text{mph}}(0)(1+z)^{n-1} \frac{dz}{H_0 E(z)}, \quad (17)$$

where $E(z) = \sqrt{\Omega_\Lambda + \Omega_M(1+z)^3}$ in a flat universe. We make this study only for the mass-selected sample because we can assume that stellar mass is additive: $M_\star(z_1) \geq M_\star(z_2)$ always for $z_1 < z_2$, and $\rho_{\text{rem}}(0, z)$ is representative of the number density of local galaxies that have undergone a disc–disc merger since redshift z . The same cannot be said for the luminosity-selected sample: here the number density of objects above a given absolute magnitude can decrease with time, as it is not generally the case that $M_B(z_1) \leq M_B(z_2)$ for $z_1 < z_2$. Using Eq. (17) for $\rho_{\text{rem}}(0, z)$ would overestimate the number of local galaxies that have undergone a merger.

Comparing ρ_{rem} with the number of $M_\star \geq 10^{10} M_\odot$ galaxies at redshift z_1 , $\rho(z_1)$, we obtain the fraction of merger remnants,

$$f_{\text{rem}}(z_1, z_2) = \frac{\rho_{\text{rem}}(z_1, z_2)}{\rho(z_1)}. \quad (18)$$

Applying Eq. (18) with the merger rate parameters of the mass sample from Table 5 and the mass functions from Pérez-González et al. (2008), we obtain $f_{\text{rem}}(0, 1) = 8^{+4}_{-3}\%$. This is a low value that increases to $f_{\text{rem}}(0, 1.5) = 15^{+9}_{-5}\%$. We take $z_2 = 1.5$ as an upper limit because our merger fraction parameterization is valid to this redshift (Sect. 6.3) and Pérez-González et al. (2008) mass functions are complete for $M_\star \geq 10^{10} M_\odot$ galaxies also up to $z \sim 1.5$. Interestingly, we infer that $f_{\text{rem}}(1.0, 1.5) = 21^{+14}_{-9}\%$, which is compatible with the fraction of bulge-dominated galaxies (E/S0/Sa) at $z \sim 1$ (López-Sanjuan et al., in prep). The pair study of Bundy et al. (2009) in GOODS-S reports f_{rem} in the range $0.4 < z < 1.4$. For $M_\star \geq 2 \times 10^{10} M_\odot$ galaxies they estimate $f_{\text{rem}}(0.4, 1.4) = 15\%\text{--}18\%$, which is in good agreement with our inferred value, $f_{\text{rem}}(0.4, 1.4) \sim 17\%$. Given that the Bundy et al. (2009) study is also sensitive to mergers between spheroids, and the mass limit in both studies is different, the quantitative agreement is remarkable.

The most important error source in our results is the uncertainty in the lower redshift bin, especially in the mass-selected

sample. We repeat our study with a higher merger fraction in this bin by a factor of two, $f_m^{\text{mph}}(z = 0.4) = 0.012$, and three, $f_m^{\text{mph}}(z = 0.4) = 0.018$. With these assumptions $f_{\text{rem}}(0, 1)$ increases to 12% and 18%, respectively. These values remain low, so our conclusions do not change.

6.4.2. Number of mergers per massive galaxy

As a complement to the previous section we calculate the number of expected disc–disc major mergers per $M_\star \geq 10^{10} M_\odot$ galaxy in a given redshift range,

$$\begin{aligned} N_m(z_1, z_2) &= \int_{z_1}^{z_2} \frac{\mathfrak{X}_m^{\text{mph}}(z)}{\rho(z)} \frac{dz}{H_0 E(z)} \\ &= \int_{z_1}^{z_2} f_m^{\text{mph}}(0)(1+z)^{n-1} \frac{dz}{T_{m,A} H_0 E(z)}. \end{aligned} \quad (19)$$

Taking Eq. (14) as the merger fraction parameterization we obtain $N_m(0, 3) = 1.2^{+0.4}_{-0.2}$. In addition, we also obtain $N_m(1, 3) = 1.0^{+0.4}_{-0.2}$, with only 0.2 disc–disc major mergers in $0 < z < 1$. The results are the same if we take Eq. (15) as the merger fraction parameterization. The previous $N_m(0, 3)$ value is lower than that inferred by Bluck et al. (2009)⁹ for $M_\star \geq 10^{11} M_\odot$ galaxies, $N_m(0, 3) = 1.8^{+0.6}_{-0.4}$, which implies that more massive galaxies have higher number of mergers than less massive ones. On the other hand, our value is ~ 4 times lower than that of Conselice (2006b); Conselice et al. (2008), $N_{\text{gm}}(0, 3) \sim 4.4$ for $M_\star \geq 10^{10} M_\odot$ galaxies. We suspect that two factors contribute to their high value. First, they use the galaxy merger fraction (f_{gm} , the fraction of galaxies undergoing mergers) to obtain $N_{\text{gm}}(z_1, z_2)$, the mean number of galaxies that merge since z_2 to obtain a z_1 galaxy. This is roughly 2 times higher than N_m (the number of merger events per galaxy). And second, they use classical counting statistics which, as shown in Sects 5 and 6.3, leads to an overestimate of the merger fraction by another factor of 2.

These results suggest that most of the disc–disc merger activity of $M_\star \geq 10^{10} M_\odot$ galaxies happened before $z \sim 1$, this kind of merger being important in galaxy evolution down to this redshift. It is important to recall that our methodology cannot detect spheroidal major mergers, so the role of these mergers in the evolution of the red sequence since $z \sim 1$ (Bell et al. 2004; Faber et al. 2007) cannot be addressed by our study. However, due to the paucity of spheroidal systems at $z \gtrsim 1.2$ (Conselice et al. 2005; Cassata et al. 2005), one expects spheroidal major mergers to be important at lower redshifts; i.e. $z \lesssim 1.2$. The simulations of Khochfar & Silk (2008) are in agreement with this picture: they find that the dry merger rate is two orders of magnitude less than the wet merger rate at $z \sim 1.5$, while they are similar at $z \sim 0.6$. In addition, they find that

⁹ We apply Eq. (19) to their best power-law fit of the merger fraction and assume, as previously, that $T_{m,A} = 0.35 - 0.6 \text{ Gyr}$.

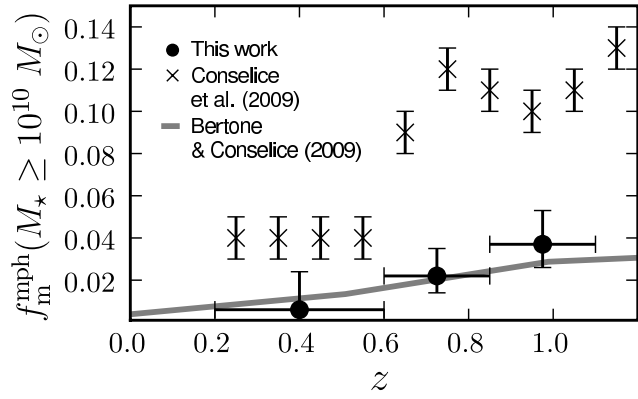


Fig. 10. Comparison between the observed and simulated merger fractions for galaxies with $M_\star \geq 10^{10} M_\odot$. The observations are from this work (black bullets), and from Conselice et al. (2009, crosses). The predictions (gray solid lines) are for major mergers with a time-scale of $T_{m,A} = 0.4$ Gyr (Bertone & Conselice 2009).

the wet merger rate has its maximum at $z \sim 1.3$, and then declines by an order of magnitude until $z = 0$, a similar evolution to our results, $\mathfrak{R}_m^{\text{mph}}(1.3) \sim 20\mathfrak{R}_m^{\text{mph}}(0)$. To check these ideas we explore the relative importance of disc–disc mergers in the structural evolution of $M_\star \geq 10^{10} M_\odot$ galaxies in a forthcoming paper.

6.5. Comparison with model predictions

The comparison of the predictions by cosmological simulations with our results is not straightforward because we only detect disk–disk (i.e. wet) major mergers, and we select by stellar mass: the simulations from Stewart et al. (2008) point out that the merger fraction depends on merger definition (minor vs major), selection criteria (halo mass, stellar mass, or luminosity) or the assumed merger time-scale.

The study from Bertone & Conselice (2009) provides predictions for major mergers of $M_\star \geq 10^{10} M_\odot$ galaxies, assuming a merger time-scale of $T_{m,A} = 0.4$ Gyr. In figure 10 we show the predictions (gray solid line), and the observational data from this work (black bullets) and Conselice et al. (2009, crosses). The predictions are in good agreement with our observations, while the Conselice et al. (2009) values are higher than predicted by factors 2 to 6. However, this agreement must be taken as qualitative more than quantitative because (i) cosmological simulations might underestimate the major merger fraction at that stellar mass, as pointed out by Bertone & Conselice (2009), (ii) the predictions are for *total* (i.e. wet + dry) major mergers, while we report wet major mergers. This can lead in a $\sim 1\%$ increase in the merger fractions due to dry mergers (Bell et al. 2006a; Lotz et al. 2008b). And, (iii) the GOODS-S merger fractions might be lower than the cosmological value due to cosmic variance (Sect. 6.1). Despite these caveats, the agreement is remarkable.

On the other hand, the simulations of Stewart et al. (2009) provide $f_{\text{rem}}(0, 2)$ for major wet mergers in $M_\star \geq 10^{10} M_\odot$ galaxies: they predict $f_{\text{rem}}(0, 2) \sim 10\% - 20\%$, in good agreement with our inferred $f_{\text{rem}}(0, 2) \sim 21^{+11}_{-7}\%$. Finally, Weinzirl et al. (2009) compare their study of $M_\star \geq 10^{10} M_\odot$ local spiral galaxies with the predictions by the Khochfar & Silk (2006) and Hopkins et al. (2009b) models. They find that both models are able to explain

the observed bulge-to-total ratio (B/T) distribution, and predict that only 13–16% of today’s $B/T < 0.75$ spirals have undergone a major merger since $z = 2$. If we assume that all the disc–disc major mergers since $z = 2$ have enough gas to re-form a disc in the merger remnant (Hopkins et al. 2009a), our $f_{\text{rem}}(0, 2) \sim 20\%$ value is an upper limit to the models’ predictions, so both are compatible with our results.

7. CONCLUSIONS

We have computed the disc–disc major merger fraction and its evolution up to $z \sim 1$ in the GOODS-S field using morphological criteria. We quantify and correct for the bias due to varying spatial resolution and image depth with redshift by artificially redshifting the galaxy images to a common reference redshift of $z_d = 1$. More importantly, we successfully account for the spillover of sources into neighbouring bins caused by the errors in asymmetry indices and in z_{phot} , through the use of an ML method developed by LGB08. In every case we obtain merger fractions lower than 0.06, in agreement with the merger fraction determination for the Groth field (L09). The main improvement in our study over previous determinations is the robust methodology that takes into account the signal-to-noise variation of galaxies with z and the observational errors: previous morphological studies using classical counts overestimate the disc–disc major merger fractions by factors of ~ 2 .

The merger fraction evolution in luminosity- and mass-selected samples are, respectively,

$$f_m^{\text{mph}}(z, M_B \leq -20) = 0.013(1+z)^{1.8}, \quad (20)$$

$$f_m^{\text{mph}}(z, M_\star \geq 10^{10} M_\odot) = 0.001(1+z)^{5.4}. \quad (21)$$

We study the effect of the LSS on these results and find that merger fractions do not change substantially.

When we compute the merger rate for both samples, the very different merger fraction evolution becomes a quite similar merger rate evolution:

$$\mathfrak{R}_m^{\text{mph}}(z) = 0.40 \times 10^{-4} (1+z)^{3.3} \text{ Mpc}^{-3} \text{ Gyr}^{-1} \quad (22)$$

for $M_B \leq -20$ galaxies and

$$\mathfrak{R}_m^{\text{mph}}(z) = 0.29 \times 10^{-4} (1+z)^{3.5} \text{ Mpc}^{-3} \text{ Gyr}^{-1} \quad (23)$$

for $M_\star \geq 10^{10} M_\odot$ galaxies. This similar evolution is due to the different number density evolution with redshift: the number of $M_\star \geq 10^{10} M_\odot$ galaxies increases with cosmic time, while the number of $M_B \leq -20$ galaxies decreases.

The previous merger rates imply that only $\sim 8\%$ of today’s $M_\star \geq 10^{10} M_\odot$ galaxies have undergone a disc–disc major merger since $z \sim 1$. Interestingly, $\sim 21\%$ of these galaxies at $z \sim 1$ have undergone a disc–disc major merger since $z \sim 1.5$, which is compatible with the fraction of bulge-dominated galaxies (E/S0/Sa) at $z \sim 1$ (López-Sanjuan et al., in prep). This suggests that disc–disc major mergers are not the dominant process in evolution of $M_\star \geq 10^{10} M_\odot$ galaxies since $z \sim 1$, with only 0.2 disc–disc major mergers per galaxy, but may be an important process at $z > 1$, with ~ 1 merger per galaxy at $1 < z < 3$.

The most important error source in these results is the uncertainty in the lower redshift bin, especially in the mass-selected sample. More studies are needed to improve the statistics at low redshift and avoid cosmic variance effects. Another important issue is the sample definition, given that merger fraction depends

on mass and luminosity: larger samples permit us different selection cuts in luminosity and mass, thus improving our knowledge of the importance of disc–disc major mergers in galaxy evolution.

Acknowledgements. We dedicate this paper to the memory of our six IAC colleagues and friends who met with a fatal accident in Piedra de los Cochinos, Tenerife, in February 2007, with particular thanks to Maurizio Panniello, whose teaching of python was so important for this paper.

We thank the anonymous referee for suggestions that improved the paper. This work was supported by the Spanish Programa Nacional de Astronomía y Astrofísica through project number AYA2006–12955, AYA2006–02358 and AYA 2006–15698–C02–02. This work was partially funded by the Spanish MEC under the Consolider-Ingenio 2010 Program grant CSD2006-00070: First Science with the GTC (<http://www.iac.es/consolider-ingenio-gtc/>). This work is based on *HST/ACS* images from GOODS *HST* Treasury Program, which is supported by NASA through grants HST-GO-09425.01-A and HST-GO-09583.01, and in part on observations made with the *Spitzer* Space Telescope, which is operated by the Jet Propulsion Laboratory, Caltech under NASA contract 1407.

P. G. P. G. acknowledges support from the Ramón y Cajal Program financed by the Spanish Government and the European Union.

References

- Abraham, R. G., van den Bergh, S., Glazebrook, K., et al. 1996, *ApJS*, 107, 1
- Adami, C., Mazure, A., Ilbert, O., et al. 2005, *A&A*, 443, 805
- Arnouts, S., Walcher, C. J., Le Fèvre, O., et al. 2007, *A&A*, 476, 137
- Balcells, M., Cristóbal-Hornillos, D., & Eliche-Moral, C. 2003, in *Revista Mexicana de Astronomía y Astrofísica*, vol. 27, Vol. 16, *Revista Mexicana de Astronomía y Astrofísica Conference Series*, ed. J. M. Rodríguez Espinoza, F. Garzon Lopez, & V. Melo Martín, 259–260
- Baldry, I. K., Glazebrook, K., Brinkmann, J., et al. 2004, *ApJ*, 600, 681
- Bekki, K., & Shioya, Y. 2001, *ApJS*, 134, 241
- Bell, E. F., Naab, T., McIntosh, D. H., et al. 2006a, *ApJ*, 640, 241
- Bell, E. F., Phelps, S., Somerville, R. S., et al. 2006b, *ApJ*, 652, 270
- Bell, E. F., Wolf, C., Meisenheimer, K., et al. 2004, *ApJ*, 608, 752
- Berrier, J. C., Bullock, J. S., Barton, E. J., et al. 2006, *ApJ*, 652, 56
- Bertone, S. & Conselice, C. J. 2009, ArXiv e-prints
- Bluck, A. F. L., Conselice, C. J., Bouwens, R. J., et al. 2009, *MNRAS*, 394, L51
- Bower, R. G., Benson, A. J., Malbon, R., et al. 2006, *MNRAS*, 370, 645
- Bridge, C. R., Appleton, P. N., Conselice, C. J., et al. 2007, *ApJ*, 659, 931
- Bundy, K., Ellis, R. S., Conselice, C. J., et al. 2006, *ApJ*, 651, 120
- Bundy, K., Fukugita, M., Ellis, R. S., Kodama, T., & Conselice, C. J. 2004, *ApJ*, 601, L123
- Bundy, K., Fukugita, M., Ellis, R. S., et al. 2009, ArXiv e-prints
- Carlberg, R. G. 1990, *ApJ*, 350, 505
- Cassata, P., Cimatti, A., Franceschini, A., et al. 2005, *MNRAS*, 357, 903
- Cassata, P., Cimatti, A., Kurk, J., et al. 2008, *A&A*, 483, L39
- Cirasuolo, M., McLure, R. J., Dunlop, J. S., et al. 2007, *MNRAS*, 380, 585
- Conselice, C. J. 2003, *ApJS*, 147, 1
- Conselice, C. J. 2006a, *MNRAS*, 373, 1389
- Conselice, C. J. 2006b, *ApJ*, 638, 686
- Conselice, C. J., Bershady, M. A., Dickinson, M., & Papovich, C. 2003, *AJ*, 126, 1183
- Conselice, C. J., Bershady, M. A., & Jangren, A. 2000, *ApJ*, 529, 886
- Conselice, C. J., Blackburne, J. A., & Papovich, C. 2005, *ApJ*, 620, 564
- Conselice, C. J., Rajgor, S., & Myers, R. 2008, *MNRAS*, 386, 909
- Conselice, C. J., Yang, C., & Bluck, A. F. L. 2009, *MNRAS*, 361
- Cowie, L. L., Songaila, A., Hu, E. M., & Cohen, J. G. 1996, *AJ*, 112, 839
- De Lucia, G. & Blaizot, J. 2007, *MNRAS*, 375, 2
- De Propriis, R., Conselice, C. J., Liske, J., et al. 2007, *ApJ*, 666, 212
- De Propriis, R., Liske, J., Driver, S. P., Allen, P. D., & Cross, N. J. G. 2005, *AJ*, 130, 1516
- Faber, S. M., Willmer, C. N. A., Wolf, C., et al. 2007, *ApJ*, 665, 265
- Fakhouri, O. & Ma, C.-P. 2008, *MNRAS*, 386, 577
- Fontana, A., Salimbeni, S., Grazian, A., et al. 2006, *A&A*, 459, 745
- Giallongo, E., Salimbeni, S., Menci, N., et al. 2005, *ApJ*, 622, 116
- Giallisco, M., Ferguson, H. C., Koekemoer, A. M., et al. 2004, *ApJ*, 600, L93
- Gottlöber, S., Klypin, A., & Kravtsov, A. V. 2001, *ApJ*, 546, 223
- Governato, F., Gardner, J. P., Stadel, J., Quinn, T., & Lake, G. 1999, *AJ*, 117, 1651
- Hopkins, P. F., Cox, T. J., Younger, J. D., & Hernquist, L. 2009a, *ApJ*, 691, 1168
- Hopkins, P. F., Hernquist, L., Cox, T. J., & Kereš, D. 2008, *ApJS*, 175, 356
- Hopkins, P. F., Somerville, R. S., Cox, T. J., et al. 2009b, ArXiv e-prints
- Hsieh, B. C., Yee, H. K. C., Lin, H., Gladders, M. D., & Gilbank, D. G. 2008, *ApJ*, 683, 33
- Jogee, S., Miller, S. H., Penner, K., et al. 2009, ArXiv e-prints
- Johansson, P. H., Naab, T., & Burkert, A. 2008, *Astronomische Nachrichten*, 329, 956
- Kampeczyk, P., Lilly, S. J., Carollo, C. M., et al. 2007, *ApJS*, 172, 329
- Kartaltepe, J. S., Sanders, D. B., Scoville, N. Z., et al. 2007, *ApJS*, 172, 320
- Khochfar, S. & Burkert, A. 2001, *ApJ*, 561, 517
- Khochfar, S. & Silk, J. 2006, *ApJ*, 648, L21
- Khochfar, S. & Silk, J. 2008, ArXiv e-prints
- Kolatt, T. S., Bullock, J. S., Somerville, R. S., et al. 1999, *ApJ*, 523, L109
- Kriek, M., van der Wel, A., van Dokkum, P. G., Franx, M., & Illingworth, G. D. 2008, *ApJ*, 682, 896
- Kuchinski, L. E., Freedman, W. L., Madore, B. F., et al. 2000, *ApJS*, 131, 441
- Lauger, S., Burgarella, D., & Buat, V. 2005, *A&A*, 434, 77
- Lavery, R. J., Remijan, A., Charmandaris, V., Hayes, R. D., & Ring, A. A. 2004, *ApJ*, 612, 679
- Le Fèvre, O., Abraham, R., Lilly, S. J., et al. 2000, *MNRAS*, 311, 565
- Lin, L., Koo, D. C., Willmer, C. N. A., et al. 2004, *ApJ*, 617, L9
- Lin, L., Patton, D. R., Koo, D. C., et al. 2008, *ApJ*, 681, 232
- López-Sanjuan, C., Balcells, M., García-Dabó, C. E., et al. 2009, *ApJ*, 694, 643 (L09)
- López-Sanjuan, C., García-Dabó, C. E., & Balcells, M. 2008, *PASP*, 120, 571 (LGB08)
- Lotz, J. M., Davis, M., Faber, S. M., et al. 2008a, *ApJ*, 672, 177
- Lotz, J. M., Jonsson, P., Cox, T. J., & Primack, J. R. 2008b, *MNRAS*, 391, 1137
- Masjedi, M., Hogg, D. W., Cool, R. J., et al. 2006, *ApJ*, 644, 54
- Miller, S. H., Jogee, S., Conselice, C., et al. 2008, in *Astronomical Society of the Pacific Conference Series*, Vol. 393, *New Horizons in Astronomy*, ed. A. Frebel, J. R. Maund, J. Shen, & M. H. Siegel, 235–+
- Oyaizu, H., Lima, M., Cunha, C. E., Lin, H., & Frieman, J. 2008, *ApJ*, 689, 709
- Papovich, C., Moustakas, L. A., Dickinson, M., et al. 2006, *ApJ*, 640, 92
- Patton, D. R. & Atfield, J. E. 2008, *ApJ*, 685, 235
- Patton, D. R., Carlberg, R. G., Marzke, R. O., et al. 2000, *ApJ*, 536, 153
- Patton, D. R., Pritchett, C. J., Carlberg, R. G., et al. 2002, *ApJ*, 565, 208
- Pérez-González, P. G., Rieke, G. H., Egami, E., et al. 2005, *ApJ*, 630, 82
- Pérez-González, P. G., Rieke, G. H., Villar, V., et al. 2008, *ApJ*, 675, 234
- Ravikumar, C. D., Puech, M., Flores, H., et al. 2007, *A&A*, 465, 1099
- Rawat, A., Hammer, F., Kembhavi, A. K., & Flores, H. 2008, *ApJ*, 681, 1089
- Ryan, Jr., R. E., Cohen, S. H., Windhorst, R. A., & Silk, J. 2008, *ApJ*, 678, 751
- Salpeter, E. E. 1955, *ApJ*, 121, 161
- Scarlata, C., Carollo, C. M., Lilly, S. J., et al. 2007, *ApJS*, 172, 494
- Somerville, R. S., Lee, K., Ferguson, H. C., et al. 2004, *ApJ*, 600, L171
- Stewart, K. R., Bullock, J. S., Barton, E. J., & Wechsler, R. H. 2008, ArXiv e-prints
- Stewart, K. R., Bullock, J. S., Wechsler, R. H., & Maller, A. H. 2009, ArXiv e-prints
- Strateva, I., Ivezić, Ž., Knapp, G. R., et al. 2001, *AJ*, 122, 1861
- Taylor-Mager, V. A., Conselice, C. J., Windhorst, R. A., & Jansen, R. A. 2007, *ApJ*, 659, 162
- Weinzirl, T., Jogee, S., Khochfar, S., Burkert, A., & Kormendy, J. 2009, *ApJ*, 696, 411
- Wild, V., Walcher, C. J., Johansson, P. H., et al. 2009, *MNRAS*, 395, 144